

Proposal of Dual-Side Transient Shaping Pulse Density Modulation for Wireless Power Transfer Systems

1st Yoshinori Akamine

Graduate School of Engineering
The University of Tokyo
Kashiwa, Japan

akamine.yoshinori24@ae.k.u-tokyo.ac.jp

2nd Ryo Matsumoto

Graduate School of Frontier Sciences
The University of Tokyo
Kashiwa, Japan

matsumoto.ryo19@ae.k.u-tokyo.ac.jp

3rd Hiroshi Fujimoto

Graduate School of Frontier Sciences
The University of Tokyo
Kashiwa, Japan

fujimoto@k.u-tokyo.ac.jp

Abstract—Wireless power transfer (WPT) has gained significant attention for its versatility and potential applications in a wide range of fields, including electric vehicles (EVs), biomedical implants, and electronic devices. To achieve high-efficiency power conversion, pulse density modulation (PDM) control, which enables soft switching, is used for power regulation. However, conventional PDM switching patterns determined solely by duty cycle can result in substantial current overshoot. This paper introduces a novel method, called Dual-Side Transient Shaping Pulse Density Modulation (Dual-Side TSPDM), for mitigating current overshoot by consistently leveraging transient response superposition within PDM control. The proposed Dual-Side TSPDM approach enables PDM control by continuously superimposing transient responses, effectively suppressing overshoot. Experimental results confirm that transient responses from the primary and secondary sides effectively cancel each other, leading to overshoot reductions of 15.4% on the primary side and 33.3% on the secondary side, while simultaneously achieving stable power control.

Index Terms—Electric Vehicle, Wireless Power Transfer, Pulse Density Modulation, Transient Response, Overshoot Suppression, Current Ripple, Oscillation, Superposition, Envelope, Power Regulation, coordinated operation

I. INTRODUCTION

Wireless power transfer (WPT) has been recognized for its versatility and convenience, with promising applications in electric vehicles (EVs) [1]–[4], biomedical implants [5], and electronic devices [6], among other fields [7], [8]. In WPT systems, achieving high-efficiency power transfer has always been a top priority. Pulse Density Modulation (PDM) is a promising approach for high-efficiency power conversion, as it enables soft switching by switching voltage polarity near current zero-crossing points, which is a significant advantage [9], [10].

However, when equally spaced pulse skipping based solely on duty cycle is applied at either the inverter or the rectifier, current ripples occur, leading to significant current peaks [11]–[14]. These peaks can increase component ratings, reduce safety margins, and raise concerns about operational safety.

Several previous studies have mentioned the ripple in PDM and the excessive peak current caused by it [9], [11]–[14].

As used in [9], it is known that reducing the minimum unit of PDM to a half-cycle can suppress ripple more effectively than conventional PDM, yet ripple and the resulting excessive current can still be problematic. Both [11] and [12] perform power conversion in WPT using PDM and address current ripple as well. Their main focus is on efficiency and losses, while detailed discussion on instantaneous excessive current is not provided. In [13], a detailed discussion is provided on the ripple and overshoot generated by PDM in WPT, and these issues are addressed by shifting the frequency or temporarily combining PWM. This approach effectively mitigates ripple and overshoot, though it compromises certain aspects such as efficiency. As presented in [14], the optimization of the PDM switching pattern has successfully suppressed current ripple and overshoot; however, the extent of this suppression has not been comprehensively detailed, requiring further quantitative discussions.

To address the issue of overcurrent caused by current ripple in PDM systems, this paper proposes Dual-Side Transient Shaping Pulse Density Modulation (Dual-Side TSPDM), which suppresses current overshoot by leveraging transient response superposition through coordinated operation of both the inverter and the rectifier. This method effectively resolves the issue of significant peak currents in PDM, enabling soft-switching power conversion without requiring higher component ratings, which were previously necessary. Moreover, this control scheme can be applied to all WPT systems equipped with active rectifiers on the receiving side.

II. STRATEGY FOR SUPPRESSING THE TRANSIENT RESPONSE OF PULSE DENSITY MODULATION

A. Current Envelope Response to a Voltage Step Input

Fig. 1 shows the configuration of the SS-type WPT system with an active rectifier on the secondary side. In this system, v_i and i_i represent the AC voltage and current, respectively, while L_i and R_i are the inductance and resistance of the i -th coil ($i = 1, 2$). C_i denotes the compensation capacitor for the

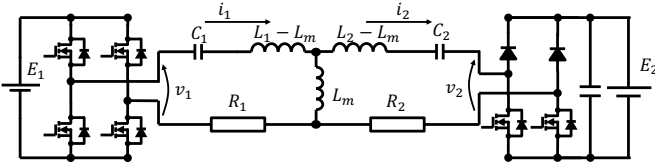


Fig. 1. SS-type WPT system with an active rectifier.

i -th coil. The mutual inductance L_m between the coils is given by:

$$L_m = k\sqrt{L_1 L_2} \quad (1)$$

where k is the coupling coefficient. Primary and secondary compensation capacitors are designed to satisfy the resonance condition of the system, as:

$$\omega = \frac{1}{\sqrt{L_1 C_1}} = \frac{1}{\sqrt{L_2 C_2}} \quad (2)$$

where ω is the angular frequency of the system. According to previous research [15], [16], The equation for the voltage/current envelope of the SS-type WPT system is expressed as follows:

$$\begin{cases} 2L_1 \frac{dI_1(t)}{dt} + R_1 I_1(t) = V_1(t) - \omega L_m I_2(t), \\ 2L_2 \frac{dI_2(t)}{dt} + R_2 I_2(t) = \omega L_m I_1(t) - V_2(t). \end{cases} \quad (3)$$

Here, $V_1(t)$ and $V_2(t)$ represent the amplitudes of the fundamental frequency voltages on the primary and secondary sides, respectively, and $I_1(t)$ and $I_2(t)$ represent the amplitudes of the fundamental frequency currents on the primary and secondary sides, respectively. In the following discussion, the amplitudes of the fundamental frequency voltages are assumed to be constant when a constant DC voltage is applied on the primary and secondary sides, such that $V_1(t) = V_1$ and $V_2(t) = V_2$.

From (3), the response of the current envelope to a step voltage input is described in the s -domain as follows [16].

$$\begin{bmatrix} I_1 \\ I_2 \end{bmatrix} = \frac{\omega_n^2}{s^2 + 2\zeta\omega_n s + \omega_n^2 + \alpha_1\alpha_2} \cdot \begin{bmatrix} \frac{1}{2L_1} \frac{1}{\omega_n^2} (s + \alpha_2) & \frac{1}{\omega L_m} \\ \frac{1}{\omega L_m} & -\frac{1}{2L_2} \frac{1}{\omega_n^2} (s + \alpha_1) \end{bmatrix} \begin{bmatrix} V_1 \\ V_2 \end{bmatrix} \quad (4)$$

The coefficients in (4) are given as:

$$\begin{cases} \alpha_1 = \frac{R_1}{2L_1}, & \alpha_2 = \frac{R_2}{2L_2}, \\ \omega_n = \frac{\omega k}{2}, & \zeta = \frac{1}{2} \left(\frac{1}{Q_1} + \frac{1}{Q_2} \right) \frac{1}{k}, \\ Q_1 = \frac{\omega L_1}{R_1}, & Q_2 = \frac{\omega L_2}{R_2}. \end{cases} \quad (5)$$

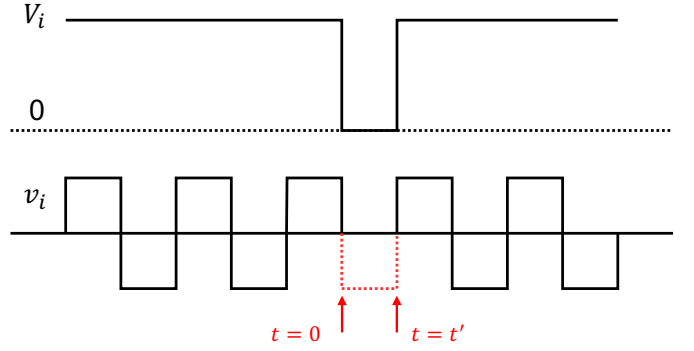


Fig. 2. The minimum unit of pulse skipping.

Given that $\omega^2 L_m^2 \gg R_1 R_2$, the approximation $\omega_n^2 + \alpha_1 \alpha_2 \approx \omega_n^2$ holds. Under this condition, (4) can be written as a standard second-order system as follows.

$$\begin{bmatrix} I_1 \\ I_2 \end{bmatrix} = \frac{\omega_n^2}{s^2 + 2\zeta\omega_n s + \omega_n^2} \cdot \begin{bmatrix} \frac{1}{2L_1} \frac{1}{\omega_n^2} (s + \alpha_2) & \frac{1}{\omega L_m} \\ \frac{1}{\omega L_m} & -\frac{1}{2L_2} \frac{1}{\omega_n^2} (s + \alpha_1) \end{bmatrix} \begin{bmatrix} V_1 \\ V_2 \end{bmatrix} \quad (6)$$

From (6), the current envelope response to a step voltage input in time domain can be expressed as follows [16].

$$I_{11\text{step}}(t) \approx \frac{V_1}{\omega L_m} \sqrt{\frac{L_2}{L_1}} e^{-\zeta\omega_n t} \sin \omega_n t \quad (7)$$

$$I_{21\text{step}}(t) \approx \frac{V_1}{\omega L_m} (1 - e^{-\zeta\omega_n t} \cos \omega_n t) \quad (8)$$

$$I_{12\text{step}}(t) \approx \frac{V_2}{\omega L_m} (1 - e^{-\zeta\omega_n t} \cos \omega_n t) \quad (9)$$

$$I_{22\text{step}}(t) \approx \frac{V_2}{\omega L_m} \sqrt{\frac{L_1}{L_2}} e^{-\zeta\omega_n t} \sin \omega_n t \quad (10)$$

Here, $I_{ij\text{step}}(t)$ represents the step response of I_i to V_j .

B. Current Envelope Response to Pulse Skipping

Fig. 2 shows the minimum unit of pulse skipping. The applied voltage in this context has only two patterns: either the DC bus voltage (or its inverse polarity) is applied, or zero voltage is applied. Here, we consider the case where the voltage application stops at $t = 0$ and resumes at $t = t'$. In PDM, to achieve soft switching, the width of the pulse skip is an integer multiple of half the operating period [9]. Using (7) – (10), the response of the current envelope to the pulse skip can be expressed as follows.

$$\begin{aligned}
I_{11\text{skip}}(t) &= -\frac{V_1}{\omega L_m} \sqrt{\frac{L_2}{L_1}} e^{-\zeta \omega_n t} \sin \omega_n t \\
&\quad + \frac{V_1}{\omega L_m} \sqrt{\frac{L_2}{L_1}} e^{-\zeta \omega_n (t-t')} \sin \omega_n (t-t') \\
&= A_{11} e^{-\zeta \omega_n t} ((e^{\zeta \omega_n t'} \cos \omega_n t' - 1) \sin \omega_n t \\
&\quad - e^{\zeta \omega_n t'} \sin \omega_n t' \cos \omega_n t) \\
&\approx -A_{11} B e^{-\zeta \omega_n t} \cos \omega_n t \tag{11} \\
I_{21\text{skip}}(t) &\approx -A_{21} B e^{-\zeta \omega_n t} \sin \omega_n t \tag{12} \\
I_{12\text{skip}}(t) &\approx -A_{12} B e^{-\zeta \omega_n t} \sin \omega_n t \tag{13} \\
I_{22\text{skip}}(t) &\approx A_{22} B e^{-\zeta \omega_n t} \cos \omega_n t \tag{14}
\end{aligned}$$

$$\begin{cases}
A_{11} = \frac{V_1}{\omega L_m} \sqrt{\frac{L_2}{L_1}}, & A_{21} = \frac{V_1}{\omega L_m}, \\
A_{12} = \frac{V_2}{\omega L_m}, & A_{22} = \frac{V_2}{\omega L_m} \sqrt{\frac{L_1}{L_2}}, \\
B = B(t') = e^{\zeta \omega_n t'} \sin \omega_n t'.
\end{cases} \tag{15}$$

In this context, $I_{ij\text{skip}}(t)$ represents the response of I_i to the pulse skip of V_j . The derivation process from (12) to (14) follows the same approach as that of (11). Note that the constant term is ignored in this analysis, as the focus is on the superposition of transient responses. However, in the derivation from (11) to (15), it is assumed that the skip width t' is sufficiently small, allowing the following approximation to hold.

$$|e^{\zeta \omega_n t'} \cos \omega_n t' - 1| \ll |e^{\zeta \omega_n t'} \sin \omega_n t'| \quad (\because t' \ll 1) \tag{16}$$

Based on the above equation, it can be concluded that the current envelope in response to the pulse skip exhibits an amplitude expressed as the product of a term dependent on circuit parameters (A_{ij}) and a term dependent on the width of the pulse skip (B).

C. Overshoot Suppression in PDM through the Superposition of Transient Responses

Fig. 3 shows the concept of Dual-Side TSPDM. T_e represents one period of the operating frequency. From the equations (11) – (15), it is necessary to apply the following switching strategy to prevent current overshoot. First, primary-side pulse skipping is performed, causing the current envelope to start oscillating in the decreasing direction. After waiting for a quarter-period of the envelope oscillation (denoted as t_d in Fig. 3), secondary-side pulse skipping is performed. By doing so, the transient responses are appropriately superimposed, cancelling the oscillation of the current envelope. The current envelope actually measured exhibits a waveform as shown by the red line in Fig. 3.

To satisfy these requirements, the transient responses induced by primary-side and secondary-side pulse skipping must have opposite phases and equal amplitudes. Based on (11) – (14), the phase condition is expressed as a constraint on t_d ,

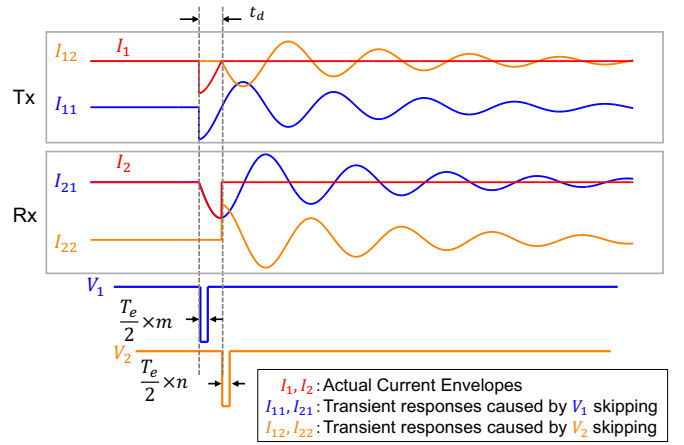


Fig. 3. The concept of Dual-Side TSPDM.

and the amplitude condition is expressed as a constraint on the skip width (m, n) and circuit parameters, as expressed in the following equations:

$$\begin{cases}
\omega_n t_d = \frac{\pi}{2}, \\
A_{11} B(\frac{T_e}{2} \times m) = A_{12} B(\frac{T_e}{2} \times n), \\
A_{21} B(\frac{T_e}{2} \times m) = A_{22} B(\frac{T_e}{2} \times n).
\end{cases} \tag{17}$$

$$\Leftrightarrow \begin{cases}
t_d = \frac{\pi}{k\omega}, \\
\frac{B(\frac{T_e}{2} \times m)}{B(\frac{T_e}{2} \times n)} = \frac{V_2}{V_1} \cdot \sqrt{\frac{L_1}{L_2}} \cdot e^{\zeta \omega_n t_d}.
\end{cases} \tag{18}$$

Since the cancellation conditions for primary-side and secondary-side current oscillations are identical, the constraint conditions are described by two equations as shown in (18). After the primary-side pulse skip corresponding to an integer m is executed, the secondary-side pulse skip corresponding to an integer n occurs with a delay of t_d . This appropriate overlapping of transient responses suppresses subsequent current oscillations. For example, if there is a significant difference in inductance between the transmitting and receiving coils and the term A_{11} is small compared to A_{12} , increasing m relative to n can bring the generated transient responses closer to the same amplitude. Hereafter, the case where the skip widths of the primary-side and secondary-side pulse skipping are $(T_e/2) \times m$ and $(T_e/2) \times n$, respectively, is referred to as the $[m:n]$ type TSPDM.

III. EXPERIMENTAL VERIFICATION

A. Experimental Setup

To evaluate the proposed control method, the experimental setup shown in Fig. 4 was constructed. The circuit configuration used is of the SS type. The controller generates switching signals for the inverter and the Semi-Bridge Active Rectifier (SBAR). The inverter produces an AC current, enabling power transfer via a magnetic field between the transmitting and receiving coils, which is then converted to DC power by the SBAR. Table I shows the parameters of the experimental setup.

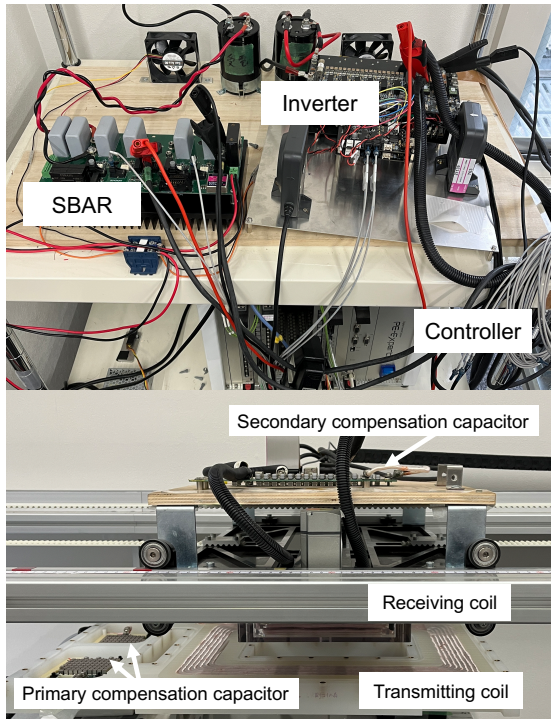


Fig. 4. Experimental setup.

TABLE I
PARAMETERS OF EXPERIMENTAL SETUP

Symbol	Definition	Value
f_o	Operating frequency	85 kHz
L_1	Transmitter inductance	131.4 μ H
R_1	Transmitter resistance	146.2 m Ω
L_2	Receiver inductance	54.8 μ H
R_2	Receiver resistance	105.2 m Ω
L_m	Mutual inductance	11.8 μ H
E_1	Transmitting-side dc-link voltage	30 V
E_2	Receiving-side dc-link voltage	33.8 V
k	Coupling coefficient	0.139

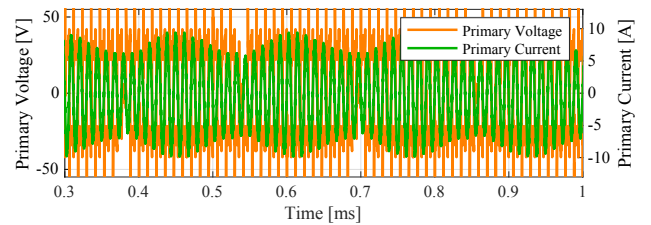
B. Conventional and Proposed PDM methods

In this study, PDM control with relatively high duty cycles was investigated. This is because, when the duty cycle is small, both transmitted and received power decrease, leading to a reduction in the average current, which in turn reduces the risk of excessive peak currents.

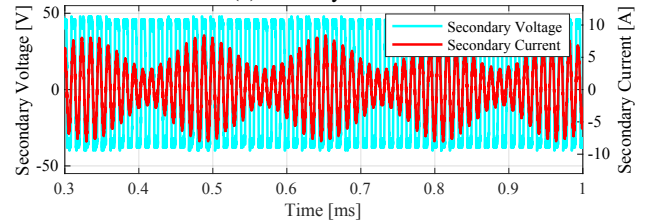
Moreover, as shown in (10), setting the secondary side to short mode causes the secondary-side current to increase stepwise instantaneously during pulse skipping. Therefore, as a comparison method, PDM control was applied only to the primary side.

To compare with the highest-resolution conventional method, we used Half-period PDM, where the smallest unit is set to half the driving frequency period. To satisfy the amplitude cancellation conditions in the proposed method, the number of skipped pulses on the primary side was set to $m = 2$, and on the secondary side to $n = 1$.

For Dual-Side TSPDM, where the same duty cycle D_{conv} , which represents the system duty cycle in conventional single-

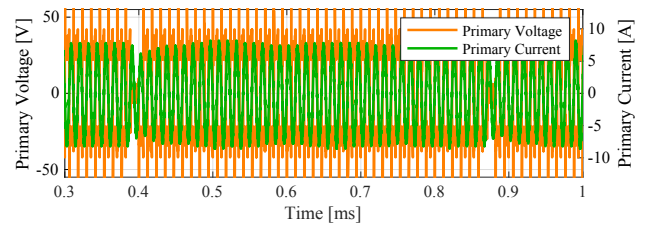


(a) Primary side.

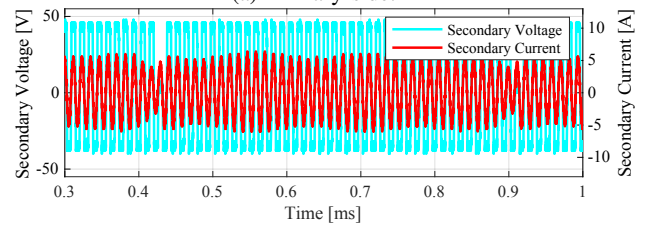


(b) Secondary side.

Fig. 5. Experimental results of Conventional Half Period PDM ($k=0.139$, Duty = 0.964).



(a) Primary side.



(b) Secondary side.

Fig. 6. Experimental results of Dual-Side TSPDM ($k=0.139$, Duty = 0.964).

side PDM, is divided between the primary and secondary sides, the total system duty cycle D_{prop} can be expressed as follows:

$$D_{\text{prop}} = D_1 \times D_2 \quad (19)$$

where D_1 and D_2 represent the duty cycles on the primary and secondary sides, respectively.

In the experiment, to achieve $D_{\text{conv}} = 27/28 \approx 0.964$, the duty cycles were set as $D_1 = 81/83 \approx 0.976$ and $D_2 = 82/83 \approx 0.988$. D_{conv} is implemented by skipping only one pulse during 28 half-cycles. The same concept applies to D_1 and D_2 . In this case, $D_{\text{prop}} = 0.976 \times 0.988 \approx 0.964$.

C. Experimental Results

Figs. 5 and 6 show the experimental results of the conventional and proposed PDM methods, respectively. From Fig.

TABLE II
COMPARISON OF MAXIMUM CURRENT VALUES,
DUTY, AND RECEIVING POWER

	Full Pulse	Half-period PDM	TSPDM
Maximum Value of I_1 [A]	7.8	9.4	8.2
Maximum Value of I_2 [A]	6.0	8.4	6.4
Overshoot of I_1 [%]	/	20.5	5.1
Overshoot of I_2 [%]	/	40.0	6.7
Duty	1.0	0.964	0.964
Receiving power [W]	112.4	108.4	108.5

5, it can be observed that pulse skipping of the primary-side voltage occurs at equal intervals, resulting in significant oscillations in the current envelope. This is because power control via PDM is performed only on one side, with the sole objective of satisfying the duty cycle constraints.

On the other hand, Fig. 6 demonstrates that the generated transient responses are effectively superimposed, leading to suppressed current peaks. More specifically, pulse skipping corresponding to $m = 2$ occurs on the primary side, followed by pulse skipping corresponding to $n = 1$ on the secondary side with a delay of $t_d = 5.88\mu\text{s} \times 7$. As a result, the phases of the transient responses due to pulse skipping on each side are approximately in opposite phase. Combined with the amplitude conditions being satisfied, this effectively suppresses the current peak values.

Table II shows the comparison of the maximum current values, duty cycles, and receiving power for the full pulse, Half-period PDM, and TSPDM methods. From Table II, it was confirmed that compared to the conventional Half-period PDM, the use of Dual-Side TSPDM reduces overshoot by 15.4% on the primary side and 33.3% on the secondary side. The received power achieved by the proposed method is almost the same as that by the conventional method, confirming that the appropriate amount of received power corresponding to the duty cycle has been successfully achieved.

IV. CONCLUSION

This paper proposed a control method to suppress excessive currents caused by current ripples in PDM. The method effectively suppresses excessive currents by superimposing transient responses generated by pulse skipping in both the inverter and the active rectifier, minimizing their impact. Using the envelope model of an SS-type equivalent circuit for voltage and current, the response model of the current envelope to pulse skipping was derived. Conditions for effectively canceling transient responses, including phase and amplitude conditions, were identified. Experiments demonstrated that the generated transient responses effectively canceled each other, achieving reductions in current overshoot by 15.4% on the primary side and 33.3% on the secondary side. Additionally, the proposed method successfully achieved PDM-based power control while ensuring the desired duty on the receiving side.

ACKNOWLEDGMENT

This work was partly supported by JST-Mirai Program Grant Number JPMJMI21E2 and JSPS KAKENHI Grant Number JP23H00175, Japan.

REFERENCES

- [1] M. Budhia, G. A. Covic, and J. T. Boys, "Design and Optimization of Circular Magnetic Structures for Lumped Inductive Power Transfer Systems," *IEEE Transactions on Power Electronics*, vol. 26, no. 11, pp. 3096–3108, Nov. 2011.
- [2] S. Li and C. C. Mi, "Wireless Power Transfer for Electric Vehicle Applications," *IEEE Journal of Emerging and Selected Topics in Power Electronics*, vol. 3, no. 1, pp. 4–17, Mar. 2015.
- [3] A. N. Azad, A. Echols, V. A. Kulyukin, R. Zane, and Z. Pantic, "Analysis, Optimization, and Demonstration of a Vehicular Detection System Intended for Dynamic Wireless Charging Applications," *IEEE Transactions on Transportation Electrification*, vol. 5, no. 1, pp. 147–161, Mar. 2019.
- [4] D. Gunji, O. Shimizu, S. Nagai, T. Fujita, and H. Fujimoto, "Greenhouse Gas Emission Evaluation Including Infrastructure for Passenger Electric Vehicles with Dynamic Wireless Power Transfer," *IEEJ Journal of Industry Applications*, Advance Publication, pp. 1–7, Mar. 2025, doi: 10.1541/ieejia.24012871.
- [5] C. Liu, C. Jiang, J. Song, and K. T. Chau, "An Effective Sandwiched Wireless Power Transfer System for Charging Implantable Cardiac Pacemaker," *IEEE Transactions on Industrial Electronics*, vol. 66, no. 5, pp. 4108–4117, May 2019.
- [6] S. Y. Hui, "Planar Wireless Charging Technology for Portable Electronic Products and Qi," *Proceedings of the IEEE*, vol. 101, no. 6, pp. 1290–1301, Jun. 2013.
- [7] T. Fujita, Y. Deguchi, and H. Fujimoto, "Impedance Analysis of Parity-Time Wireless Power Transfer System using Digital Separate-Oscillation," *IEEJ Journal of Industry Applications*, vol. 13, no. 6, pp. 703–710, Nov. 2024.
- [8] R. Matsumoto and H. Fujimoto, "Adaptive Compensation Scheme for Wireless Power Transfer Systems with Coil Inductance Variation Using PWM-Controlled Switched Capacitor," in *Proc. IEEE Wireless Power Week (WPW)*, pp. 244–248, 2022.
- [9] V. Esteve, J. Jordán, E. Sanchis-Kilders, E. J. Dede, E. Maset, J. B. Ejea, and A. Ferreres, "Enhanced Pulse-Density-Modulated Power Control for High-Frequency Induction Heating Inverters," *IEEE Transactions on Industrial Electronics*, vol. 62, no. 11, pp. 6905–6914, Nov. 2015.
- [10] H. Li, J. Fang, S. Chen, K. Wang, and Y. Tang, "Pulse Density Modulation for Maximum Efficiency Point Tracking of Wireless Power Transfer Systems," *IEEE Transactions on Power Electronics*, vol. 33, no. 6, pp. 5492–5501, June 2018.
- [11] V. Yenil and S. Cetin, "An Improved Pulse Density Modulation Control for Secondary Side Controlled Wireless Power Transfer System Using LCC-S Compensation," *IEEE Transactions on Industrial Electronics*, vol. 69, no. 12, pp. 12762–12772, Dec. 2022.
- [12] J. Tang, T. Na, and Q. Zhang, "A Novel Full-Bridge Step Density Modulation for Wireless Power Transfer Systems," *IEEE Transactions on Power Electronics*, vol. 38, no. 1, pp. 41–45, Jan. 2023.
- [13] J. Zhou, G. Guidi, K. Ljokelsoy, and J. A. Suul, "Evaluation and Suppression of Oscillations in Inductive Power Transfer Systems With Constant Voltage Load and Pulse Skipping Modulation," *IEEE Transactions on Power Electronics*, vol. 38, no. 8, pp. 10412–10425, Aug. 2023.
- [14] J. Zhou, G. Guidi, S. Chen, Y. Tang, and J. A. Suul, "Conditional Pulse Density Modulation for Inductive Power Transfer Systems," *IEEE Transactions on Power Electronics*, vol. 39, no. 1, pp. 88–93, Jan. 2024.
- [15] H. Li, J. Fang, and Y. Tang, "Dynamic Phasor-Based Reduced-Order Models of Wireless Power Transfer Systems," *IEEE Transactions on Power Electronics*, vol. 34, no. 11, pp. 11361–11370, Nov. 2019.
- [16] T. Hamada, T. Fujita, and H. Fujimoto, "Fast Start-Up Control of Both-Side Current Without Overshoot Focusing on Rectification Timing for Dynamic Wireless Power Transfer Systems," *IEEE Journal of Emerging and Selected Topics in Industrial Electronics*, vol. 5, no. 3, pp. 1039–1047, Jul. 2024.